*Journal of Sound and Vibration* (2000) **231**(5), 1311–1320
doi:10.1006/jsvi.1999.2732, available online at http://www.idealibrary.com on IDEAL®

# MEASURED FREE VIBRATIONS OF PARTIALLY CLAMPED, SQUARE PLATES

J. F. WILSON

*Department of Civil and Environmental Engineering, Duke University, Durham, NC 27708-0287, U.S.A.*

AND

J. K. HENRY AND R. L. CLARK

*Department of Mechanical Engineering and Material Science, Duke University, Durham, NC 27708-0300, U.S.A.*

(*Received* 28 *January* 1999, *and in final form* 11 *October* 1999)

Experiments were designed to measure the free, transverse vibrations for square, thin elastic plates with two types of edge support configurations. One configuration was fully clamped on three edges and free on the fourth edge (CCCF), and the other was fully clamped on two adjacent edges and free on the other two edges (CCFF). For these respective configurations, up to 18 frequencies and the corresponding modal contours were measured using a scanning laser-doppler velocimeter, acoustic excitation, and computer software. Measurements for the lowest five non-dimensional frequency parameters $\lambda$ and their node lines compared favorably to the corresponding theoretical results available in the open literature. Curve veering may be the reason that several of the crisp modal contours at some higher excitation frequencies for the CCFF configuration were observed to be neither symmetric nor antisymmetric about the plate's diagonal line of geometric symmetry.


## 1. INTRODUCTION

One of the bases of comparison between experimental and theoretical results for the free, transverse, harmonic vibrations of classical plates is the non-dimensional frequency parameter $\lambda$. This parameter, which appears as a coefficient in the non-dimensional form of this plate's governing fourth order differential equation [1], is

$$\lambda = \omega a^2 \sqrt{\frac{\rho}{D}}. \tag{1}$$

Here, $\omega$ is the plate frequency (rad per unit time), $a$ is the dimension of the sides, $\rho$ is the mass density per unit of surface area, and $D$ is flexural stiffness given by

$$D = \frac{Eh^3}{12(1-\nu^2)}. \tag{2}$$

0022-460X/00/151311 + 10 $35.00/0 

In the last equation, $E$ is Young's modulus, $h$ is the thickness dimension, and $v$ is the Poisson ratio for the plate.

An exhaustive summary of the open literature on both theoretical and experimental measures of $\lambda$ for various plate geometries under a variety of constraints was published by Leissa [1] in 1968 and articles of such measurements continue to be published in *Experimental Mechanics*. Such measurements have employed a variety of techniques, including electrodynamic plate excitation in which resonance frequencies were identified by distinct increases in noise levels [2]; node visualization using Moire–Salet–Ikeda methods [3]; and holographic interferometry [4]. Unlike these classical experimental studies, the present study employs state-of-the-art scanning laser doppler velocimeter, acoustic plate excitation, and computer software to interpret the plate vibration data and display the modal contours.

Shown in Figure 1 are the two plate configurations considered herein, for which no previous experimental studies were found. Figure 1(a) defines the first configuration: a square plate clamped on three sides and free on the fourth, designated CCCF. This configuration was first studied theoretically by Elsbernd and Leissa [5], who used the Ritz method with products of beam deflections

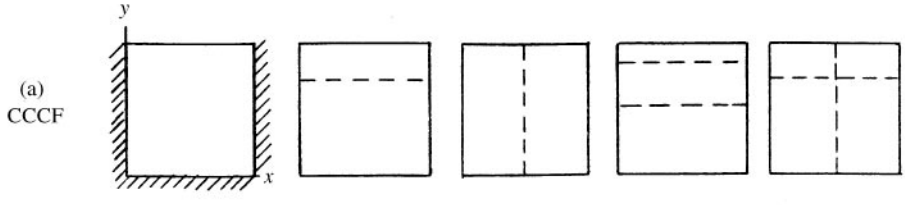


| | $\lambda_{11}$ | $\lambda_{12}$ | $\lambda_{21}$ | $\lambda_{13}$ | $\lambda_{22}$ |
|---|---|---|---|---|---|
| Theory [5]: | 24·010 | 40·030 | 63·440 | 76·740 | 80·700 |
| Theory [6]: | 24·020 | 40·039 | 63·493 | 76·761 | 80·713 |
| Experiment | 24·000 | 39·400 | 67·100 | 77·500 | 77·800 |

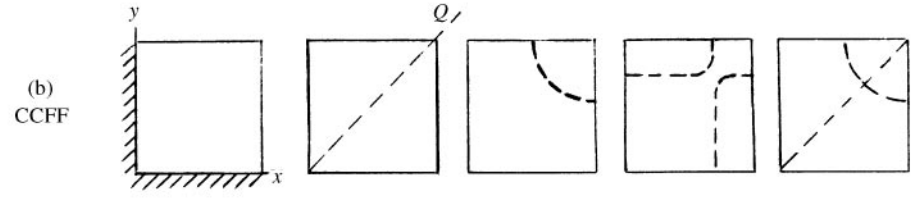


| | $\lambda_{11}$ | $\lambda_{21}$ | $\lambda_{12}$ | $\lambda_{22}$ | $\lambda_{13}$ |
|---|---|---|---|---|---|
| Theory [9]: | 6·9580 | 24·800 | 26·800 | 48·050 | 63·140 |
| Theory [6]: | 6·9421 | 24·034 | 26·681 | 47·785 | 63·039 |
| Experiment | 6·7700 | – | 26·200 | 47·200 | 58·400 |

Figure 1. A summary of the theoretical frequency parameters $\lambda$ and their corresponding nodal (dashed) lines: (a) the CCCF square plate, and (b) the CCFF square plate. The sixth lowest theoretical values are $\lambda = 116{\cdot}8$ for the CCCF and $\lambda = 65{\cdot}83$ for the CCFF configuration [6]. The first four measured values of $\lambda$ are also given, and their corresponding modal contours may be seen in Figures 3 and 4.

functions, to compute theoretical values for the lowest five values for $\lambda$ and their corresponding nodal patterns, both given in Figure 1(a). Figure 1(b) defines the second configuration: a square plate clamped on two adjacent sides and free on the other two, designated CCFF. The theoretical results for the latter configuration, also based on the Ritz method using beam functions, were reported in references [6–9], of which results in references [6] and [9] appear to be the most accurate. Their five lowest theoretical values of $\lambda$ and their nodal patterns are given in Figure 1(b). For both the CCCF and the CCFF configuration, Leissa [6] subsequently reported the respective theoretical values of the sixth lowest frequency parameters, which are listed in Figures 1(a) and 1(b) for comparison purposes; however, the latter reference did not report the corresponding nodal lines for either configuration. Related studies include those of Groves and Clark [10], who presented insights into the choice of trial functions for predicting $\lambda$ for higher, antisymmetric modes. Further, Leissa [11] studied the phenomenon of curve veering in plate vibrations, previously discussed by Classen and Thorne [12], a theoretical prediction (based on approximations) that two different modal shapes with equal or nearly equal frequencies may exist for a plate with an aspect ratio at or close to unity. This phenomenon is further discussed herein as it may explain some of the unexpected and non-intuitive experimental results for the CCFF configuration that is, at several of the higher frequencies, crisp modal contours were observed which were neither purely symmetric nor purely antisymmetric about the plate's geometric line of symmetry.

The purposes of the present investigation were three-fold: (1) to validate experimentally the published theoretical results (the first six $\lambda$ values and their modal contours) for the two plate configurations of Figure 1; (2) to measure for these two plate configurations the first 18 or so frequency parameters and their respective modal contours; and (3) to determine the accuracy and practicality of the experimental approach utilizing a laser–doppler velocimeter for measuring the higher frequencies of plates. What follows is a brief description of the experimental equipment and methods, a discussion of the experimental results, and conclusions about the investigation.

## 2. EXPERIMENTAL METHOD

Overall views of the experimental system are shown in Figures 2(a) and 2(b). The design of the plates' mechanical boundary constraint system for the CCCF configuration is shown in Figure 2(a), in which, for the CCFF configuration, the steel "picture" frame on the right side that bolts the experimental plate to the welded steel I-beam frame, is omitted. The major components of the experimental system are shown in Figure 2(b). Here, the speaker used for acoustic excitation of the plate (in the vertical plane) was placed at about a 45° angle to the plate face to avoid acoustic coupling of the speaker to the air column between the speaker and the plate.

The material and geometric characteristics of the four aluminium plates used in these experiments are given in Table 1. A pair of plate geometries was designed for

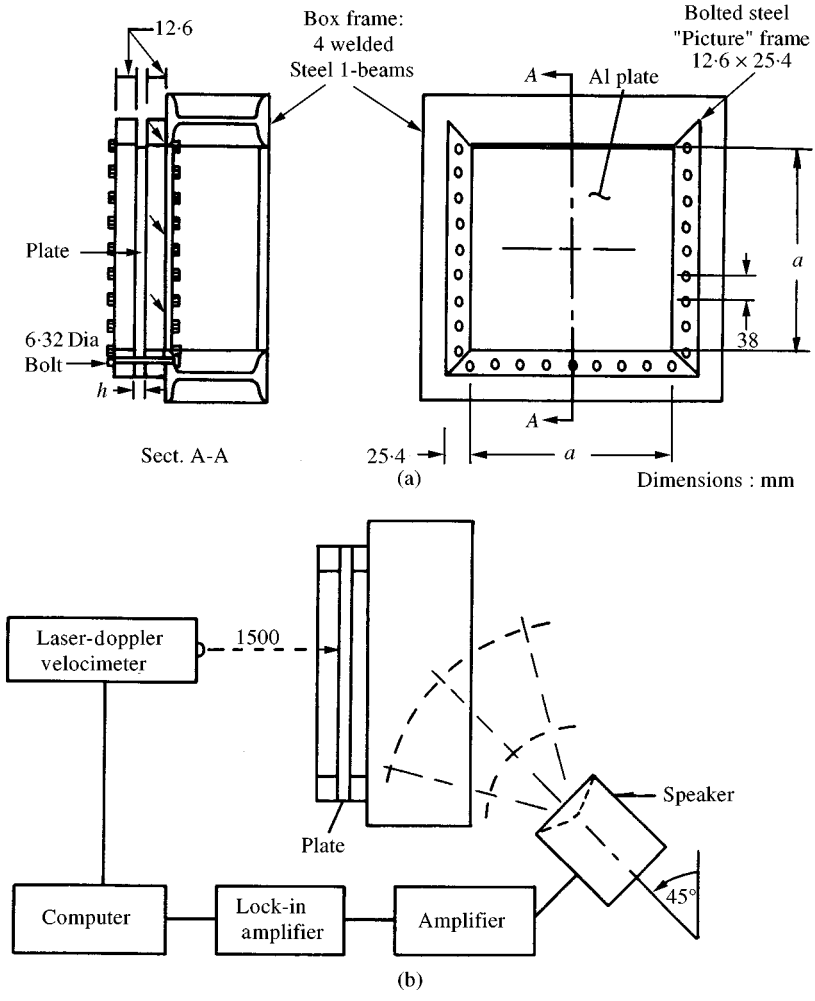


Figure 2. The experimental system: (a) plate frame design illustrating the CCCF configuration, and (b) plan view of the overall setup.

each of the two constraint configurations so that the whole range of plate free vibration frequencies, from the lowest to about the 20th, was spanned for each pair. Thus, both the frequency range (50–800 Hz) and energy output limitations of the speaker used for acoustic plate excitation were observed.

Initially, the resonance frequencies $f$(Hz) of the plate were determined by measuring frequency response functions between a broadband acoustic excitation and several point velocity outputs. The plate was then excited acoustically at each of these premeasured resonance frequencies using the lock-in amplifier and speaker system. By phase-referencing the measured velocity to that of the drive signal, the corresponding mode shape was resolved. The discrete velocity measurements required to measure the mode shapes were obtained using a Ometron VPI 4000 Scanning Laser–Doppler Velocimeter. This laser system is a non-contacting velocity transducer that measures the Doppler frequency shift at each point on a dense grid covering the surface of the plate and converts it to velocity. The

TABLE 1

*Material and geometric characteristics of the four experimental plates. The frequency multiplier C* ($Hz^{-1}$) *is based on these characteristics, and is computed from equation* (4)

| Aluminum, type 3003; $E = 68{\cdot}9$ GPa; $\nu = 0{\cdot}3$; $\rho/h = 2{\cdot}7 \times 10^3$ kg/m$^3$ | | | | |
|---|---|---|---|---|
| Plate no. | Plate constraint | Length, width $a$ (mm) | Thickness $h$ (mm) | Frequency multiplier $C$ ($Hz^{-1}$) |
| 1 | CCCF | 457 | 2·24 | 0·383 |
| 2 | CCCF | 457 | 4·85 | 0·180 |
| 3 | CCFF | 457 | 2·24 | 0·383 |
| 4 | CCFF | 305 | 3·10 | 0·123 |

software accompanying this laser system allows for the measurement of the velocity profile of a plate vibrating at a resonance frequency $f$.

The relationship between the measured value of $f$ and the non-dimensional frequency parameter $\lambda$ is derived as follows. For $\omega$ of equation (1) in the units of rad/s, $\omega = 2\pi f$. When $\omega$ and $D$ of equation (2) are substituted into equation (1), the result is

$$\lambda = Cf \tag{3}$$

in which the frequency multiplier, based only on the plate's material and geometry, is given by

$$C = 2\pi a^2 \sqrt{\frac{12(1-\nu^2)\rho}{Eh^3}}. \tag{4}$$

Numerical values of $C$ for the four experimental plates are given in Table 1. The reported values for $\lambda$ in the next section are based on these values of $C$ and the measured values of $f$.

## 3. EXPERIMENTAL RESULTS AND DISCUSSION

The measured values of $\lambda$ and their corresponding modal plots (mode shapes) are given in Figure 3 for the CCCF configuration and in Figures 4 and 5 for the CCFF configuration. In these figures, the orientations of the plates, their boundaries, and their $(x, y)$ co-ordinate system are those of Figures 1(a) and 1(b). In these experiments, the value of $f$ was measured to three significant figures, the same accuracy as that reported for $\lambda$. For the contour plots of Figures 3–5, the peak root-mean-square (r.m.s) amplitudes of transverse plate velocity were typically in the range of 5–15 mm/s for the lightest (white) areas, 1–4 mm/s for the medium gray areas and zero, or nearly so, for the black-most areas which correspond to the nodal "lines" and the clamped edges. For plots with more than one white area, a given white area was measured to be always 180° out of phase with its nearest neighbors. Since the plate motion is harmonic, the r.m.s. amplitude of plate

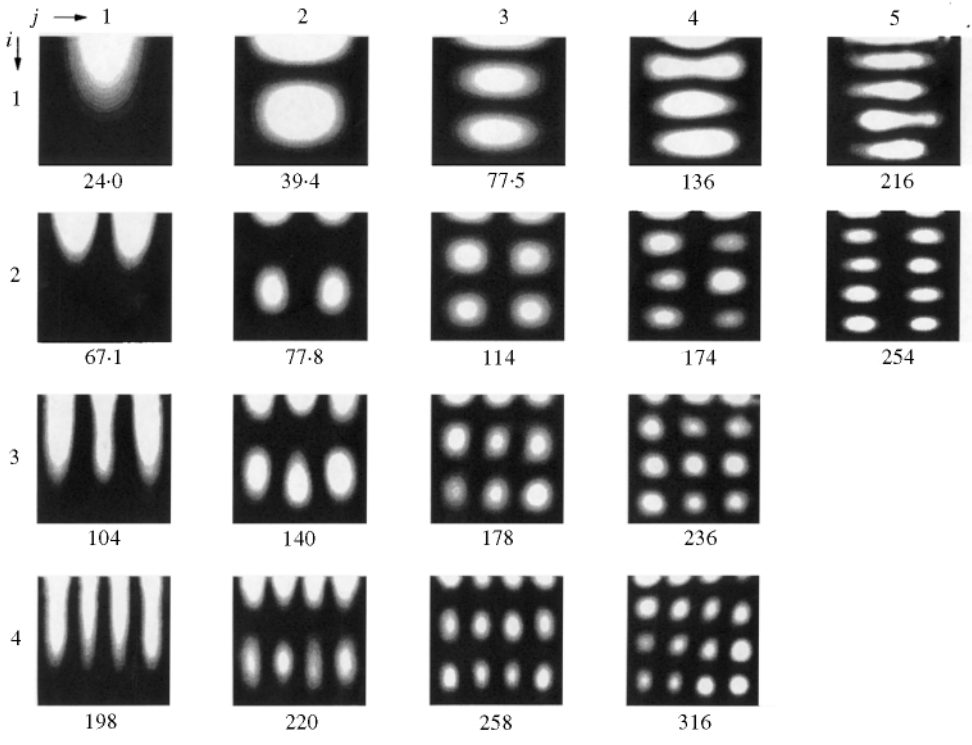


Figure 3. The CCCF plate: measured values for the frequency parameters and their corresponding modal contours, which are either symmetrical or antisymmetrical about the plate's centerline, $x = a/2$.

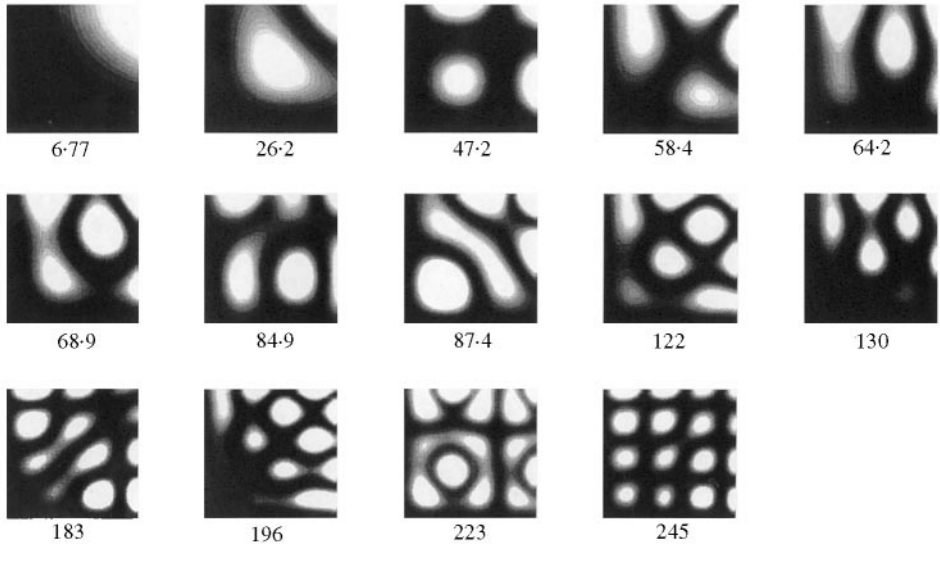


Figure 4. The CCFF plate: measured values for the frequency parameters and their corresponding modal contours, which are either symmetrical and antisymmetrical about the plate's diagonal line, Q.

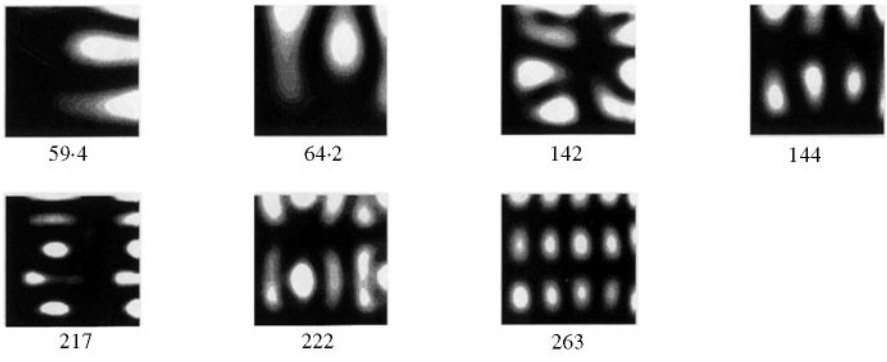


Figure 5. The CCFF plate: measured values for the frequency parameters and their corresponding modal contours, which lack symmetry about the plate's diagonal line, Q.

deflection contour plots are exactly analogous to the velocity contour plots shown. Also generated but not shown herein were the color-coded contour plot counterparts of each plot shown in Figures 3–5.

Consider the experimental results for the CCCF configuration summarized in Figure 3. Let each numerical entry for the frequency parameter have the designation $\lambda = \lambda_{ij}$ in which $i$ is its row and $j$ is its column position. For $i = 1$ and 3, the mode shapes (white areas) are symmetrical about the line of the plate's geometric symmetry, $x = a/2$ and for $i = 2$ and 4, the mode shapes are antisymmetrical about $x = a/2$. The comparisons of the first five measured nodal patterns (mean straight lines along the black areas between the white areas) with the corresponding broken node lines of Figure 1(a) used in the theoretical calculations, are excellent, as are the first, second, and fifth theoretical frequency parameters $\lambda$, which are higher than the respective measured ones, as one would expect since the Ritz method predicts an upper bound value. Why the predicted values for $\lambda_{21} = 63{\cdot}44$ and $\lambda_{13} = 76{\cdot}14$ are both somewhat lower than their respective measured values of 67·1 and 77·5 is not clear; but since crisp modal contour plots for these latter two cases were more difficult to obtain experimentally than most of the other ones of Figure 3, these discrepancies may be due more to experimental inaccuracies (discussed later) than to theory. Further, the sixth lowest value was predicted by Leissa [6] as $\lambda = 116{\cdot}8$. This upper-bound value compares well to the measured value of $\lambda_{23} = 114$, for which the measured modal contours were antisymmetrical with respect to the plate's line of symmetry, $x = a/2$.

Consider the experimental results for the CCFF configuration summarized in Figure 4. Listed are the frequency parameters and their modal contour plots: 11 symmetrical and 3 antisymmetrical about the diagonal line Q, the line of geometric symmetry for the plate. The comparisons of the first, third, fourth, and fifth theoretical values of $\lambda$ listed in Figure 1(b), as well as their corresponding nodal lines, with the respective first through fourth measured values of Figure 4, are excellent. The sixth lowest value predicted by Leissa [6] was $\lambda = 65{\cdot}83$, which corresponds to the measured value of $\lambda = 64{\cdot}2$, the fifth from the lowest and the

fourth symmetrical modal contour plot shown in Figure 4. Consistent with the Ritz method used in the theoretical calculations, all five theoretical values for $\lambda$ are close to but somewhat greater than their measured counterparts.

Repeated efforts to measure the second theoretical value of $\lambda = 24{\cdot}80$, together with its antisymmetrical modal contours, were unsuccessful. This lack of success was probably due to the unavoidable manufacturing imperfections or eccentricities in the experimental plates such as slight out-of-squareness and imperfect edge constraints and also to some non-uniformity in the acoustic excitation set forth by the speaker. At this lowest unmeasured antisymmetrical mode, such factors probably prevented the formation of a stationary diagonal line Q, especially at and near the intersection of the two free edges, the most flexible portion of the plate. In fact, in practice this first antisymmetrical mode may be physically impossible to observe without restraining the corner at the intersection of the two free edges (which was not done). However, system imperfections did not prevent the measurements for higher antisymmetrical modes, those corresponding to $\lambda = 58{\cdot}4$, 183, and 196.

Further experimental results for the CCFF configuration are the seven modal contour plots displayed in Figure 5. The plot for $\lambda = 64{\cdot}2$ of Figure 4 is repeated in Figure 5 for comparison purposes. The first observation is that the latter somewhat blurred plot appears to be nearly symmetric about the diagonal, with its two and a quarter "circles" along Q. Actually, this contour plot may not correspond to a "pure" resonance condition, but may be one in transition to the crisp plot for $\lambda = 68{\cdot}9$ in Figure 4. The second observation comes about by grouping the first six values of $\lambda$ in Figure 5 in consecutive pairs: (59·4, 64·2), (142, 144), and (217, 222), now defined as close pairing. (The second of the pair for $\lambda = 263$ could not be measured because its corresponding frequency exceeded the capacity of the apparatus.) Note that the modal contour plot for any member of a close pair is approximately the mirror image across the diagonal Q of that for the other member of pair.

The non-intuitive, non-symmetrical contours of Figure 5 may be the consequence of the "aberration phenomenon' or "curve veering" observed in theoretical studies [11] and [12] for (nearly) square membranes and plates, in which the approximate Ritz method and approximate beam mode shapes were superimposed to achieve the free vibration solutions. We paraphrase Leissa's observations on curve veering, which he attributes to the use of these approximate methods [11]: *Theoretical results for the aspect ratio R of a plate or membrane, when plotted against frequency, show that each curve for a given mode shape is well behaved, except when two such curves approach a crossing at* $R = 1$. *Instead of crossing at* $R = 1$, *these two curves veer away from each other, with the result that one mode shape is (gradually) changed to the other*. We speculate that such modal degeneracy (equal frequencies) may be the largest factor leading to the observed non-symmetric modes of Figure 5. The experimental plate is, after all, an approximation to an ideal square; the excitation frequency is an approximation to an ideal constant value and the clamped edge constraints may change ever so slightly during forced excitation, which may change the plate's aspect ratio ever so slightly during the experiment. Thus, it is not too surprising that what appears to be curve veering in approximate

theory may also be curve veering in these approximate experiments. That is, for a nearly constant excitation frequency, the electronics take a time average of the two detected modal forms, which may veer in time from diagonally symmetric to diagonally antisymmetric, or *vice versa*, to produce each non-symmetric form of Figure 5. The fact that a non-symmetric form has a minor image for paired frequencies may support the experimental existence of curve veering and the frequency between each paired frequency may be the experimental "transition zone" observed in approximate theory [12]. However, such issues need further theoretical and experimental investigation and are well beyond the scope of the present study.

## 4. SUMMARY AND CONCLUSIONS

Some items of practical interest to an experimentalist are summarized. First, even with a carefully designed experimental plate system in which geometric and other eccentricities are minimized, one may encounter curious results such as those observed for the CCFF configuration: a few modal contours corresponding to resonances that were neither symmetrical nor antisymmetrical about the diagonal line of plate symmetry. The latter results may be degenerate modes (equal frequencies) with curve veering. Second, for the available frequency range of 50–800 Hz for the present state-of-the-art system, several square plates of the same face dimensions but of different thicknesses are needed to accurately measure to three significant figures the lowest 15–20 free vibration frequency parameters $\lambda$ and their corresponding modal contours. With the equipment in place, such a study for a given plate configuration may be accomplished by an experienced experimentalist in about a day's time.

These experimental results suggest two topics that warrant further investigation. First, experimental and theoretical studies may be done on the contour patterns that are formed in the approach, at increasing excitation frequency, to a resonance state: a crisp modal contour corresponding to a free vibration frequency. For instance, by carefully observing in Figure 4 the consecutive modal contours from $\lambda = 64{\cdot}2$–$87{\cdot}4$, one may imagine the progressive formation of modal patterns as the white areas split, coalesce, expand, and migrate over the plane. Second, curve veering could be investigated using several different plates with aspects ratios near unity.

Thus, these experimental investigations show both the hazards and advantages of employing a scanning laser–doppler velocimeter, acoustic excitation, and computer software to measure and visualize the free transverse vibration characteristics of elastic plates. For the CCCF and the CCFF plate configurations used in these studies, the experimental results for the first five modal contours agreed with those reported in the open literature and the corresponding frequency parameters, experimental and theoretical, agreed to within a few percent. These results serve to validate the effectiveness, accuracy, and reliability of the present measuring system and thus give credibility to the higher frequency parameters for the CCCF and for the CCFF configurations measured in this study.

## ACKNOWLEDGMENTS

The authors greatly appreciate the contributions of Daniel P. Batt and Vivek Padmanabhan who aided in the early mechanical designs of the test plates and conducted preliminary experiments.

## REFERENCES

1. A. W. Leissa 1969 *NASA SP*-160. Vibration of plates.
2. M. E. Raville and C. E. S. Ueng 1967 *Experimental Mechanics* **7**, 490–493. Determination of natural frequencies of a sandwich plate.
3. C. R. Hazell and R. D. Niven 1968 *Experimental Mechanics* **8**, 225–231. Visualization of nodes and antinodes in vibrating plates.
4. R. C. Sampson *Experimental Mechanics* 1970 **10**, 313–320. Holographic-interferometry application in experimental mechanics.
5. G. F. Elsbernd and A. W. Leissa 1970 *Developments in Theoretical and Applied Mechanics* 19–28. Free vibration of a rectangular plate clamped on three edges and free on the fourth edge.
6. A. W. Leissa 1973 *Journal of Sound and Vibration* **31**, 257–293. The free vibration of rectangular plates.
7. J. Nagaraja and S. S. Rao 1953 *Journal of Aeronautical Science* **20**, 855–856. Vibration of rectangular plates.
8. M. Stanisic 1957 *Journal of Aeronautical Science* **24**, 159–160. An approximate method applied to the solution of the problem of vibrating rectangular plates.
9. D. Young 1950 *Journal of Applied Mechanics* **17**, 448–453. Vibration of rectangular plates by the Ritz method.
10. R. S. Groves and R. L. Clark 1998 *Journal of Sound and Vibration* **217**, 579–584. Comments on the natural frequencies of rectangular plates derived from the Raleigh–Ritz method.
11. A. W. Leissa 1974 *Journal of Applied Mathematical and Physics* (*ZAMP*) **25**, 99–111. On a curve veering aberation.
12. R. W. Classen and C. J. Thorne 1962 *Journal of Aerospace Science* **29**, 1300–1305. Vibrations of a rectangular cantilever plate.